International Journal of Thermal Sciences 48 (2009) 1949–1959

Contents lists available at ScienceDirect

International Journal of Thermal Sciences

journal homepage: www.elsevier.com/locate/ijts

Study of the heat transfer characteristics in turbulent combined wall and offset jet flows

E. Vishnuvardhanarao [1], Manab Kumar Das *

Department of Mechanical Engineering, Indian Institute of Technology Guwahati, Guwahati 781039, Assam, India

ARTICLE INFO

Article history:
Received 3 May 2008
Received in revised form
2 February 2009
Accepted 24 February 2009

Keywords:
Turbulent flow
High Reynolds number
Dual-jet flow
Computation

ABSTRACT

The heat transfer study of a combined wall jet and offset jet flow with different wall jet and offset jet flow velocities are considered. The flow is considered two-dimensional, steady, incompressible, turbulent at high Reynolds number with negligible body forces. The streamline curvature modification of the standard k–ϵ model is used to carry out the turbulence modeling. The Reynolds number is varied from 10^4 to 4×10^4 and $Pr = 0.71$ is taken for all computations. Constant wall temperature and constant wall heat flux boundary conditions are considered. The results are presented in the form of local Nusselt number, local heat flux, surface temperature in case of constant heat flux condition, average Nusselt number and total heat transfer.

1. Introduction

In case of an offset jet, the fluid issues above a wall obstruction and parallel to the axis of the jet. If the offset height is zero, the offset jet becomes a wall jet [1]. Asymmetric entrainment on both sides of the jet causes the jet to deflect towards the plate and finally attaches to it. This is called the Coanda effect [2]. Many practical applications of jet flows may be found which include the entrainment and the mixing process in a gas turbine and boiler combustion chambers, heat exchangers, fluid injectors and carburetor systems, environmental dischargers, cooling systems and many others.

The wall jet and offset jet cases are mainly studied separately. The turbulent wall jet has been studied in details by many researchers and reported in literature. These include the articles of Bakke [3], Schwarz and Cosart [4], Wygnanski et al. [5], Launder and Rodi, [6], Eriksson et al. [7], Venås et al. [8], Gogineni and Shih [9] and George et al. [10] etc. For the offset jet, the relevant articles are Pelfrey and Liburdy [11], Koo and Park [12], Pelfrey and Liburdy [13], Gu [14], Sawyer [15,16], Nasr and Lai [17]. However, the case of a combined jet flows have rarely been studied. The following experimental work of two parallel jets are reported by Ko and Lau [18], Lin and Sheu [19] and Nasr and Lai [20]. Numerical work reported are by Soong et al. [21], Anderson and Spall [22], Wang et al. [23].

A thorough literature survey reveals that research on the fluid flow and heat transfer on the combination of jets have been concentrated on two parallel plane jets. Recently Wang and Tan have experimentally studied the fluid flow behavior of the effect of a wall jet and an offset jet [24]. The schematic diagram of the dual jet is shown in Fig. 1. Wang and Tan have considered an offset ratio of $d/h = 1.0$ and done the measurements using Particle Image Velocimetry (PIV). Statistical characteristics of the flow are obtained through ensemble averaging of 360 instantaneous velocity fields. A similarity profile has been obtained and plotted. The jet half-widths at various shear layers have been plotted. Results reveal that close to the jet issuing plate, a vortex shedding has been observed.

Shuja et al. [25] have studied the turbulent jet impingement on a surface having a constant heat flux over a limited area. Air is considered as the impinging gas, and the process is simulated with a two-dimensional axisymmetric form of the governing conservation equations. Aldabbagh and Sezai [26] have investigated numerically the steady-state flow and heat transfer characteristics of impinging laminar square twin jets. The simulations have been carried out for various jet-to-jet spacings and nozzle exit-to-plate distances. Heat transfer from a row of turbulent jets impinging on a stationary surface is investigated numerically by

* Correspondence to: Manab Kumar Das, Department of Mechanical Engineering, Indian Institute of Technology Kharagpur, West Bengal 721302, India. Tel.: +91 3222 282924; fax: +91 3222 282278.

E-mail addresses: vishnu.kavuluru@gmail.com (E. Vishnuvardhanarao), manab@mech.iitkgp.ernet.in (M.K. Das).

[1] Fluidyn Software and Consultancy Pvt. Ltd, Bangalore 560 102, India.

1290-0729/$ – see front matter © 2009 Elsevier Masson SAS. All rights reserved.
doi:10.1016/j.ijthermalsci.2009.02.020

Nomenclature

$C_{1\epsilon}$, $C_{2\epsilon}$,	turbulence model constants.
E	integration constant, refer Eq. (24)
h	width of the jet
h_c	heat transfer coefficient
d	distance between the wall jet and offset jet
k	turbulent kinetic energy
Nu	Nusselt number
$\overline{Nu}$	average Nusselt number
OR	Offset ratio
$\overline{p}$	static pressure
p_0	ambient pressure
$\overline{P}$	non-dimensional static pressure
Pr	Prandtl number
Pr_t	turbulent Prandtl number
q_x, $q_{x,\,n}$	dimensional and non-dimensional local heat flux
Q	average non-dimensional heat transfer
Re	Reynolds number, U_0h/ν
$\overline{T}_w$	dimensional mean temperature
T_∞	free stream temperature
U_w	average inlet wall jet velocity
U_o	average inlet offset jet velocity
U_0	Reference jet velocity (either U_w or U_o, whichever is maximum compared to the other).
$\overline{u}, \overline{v}$	dimensional mean velocities in x, y-directions respectively
$\overline{u}$	dimensional mean temperature
$\overline{U}, \overline{V}$	non-dimensional velocities in X, Y-directions respectively
x, y	dimensional co-ordinates
X, Y	non-dimensional co-ordinates

Greek symbols

α, α_t	laminar and turbulent thermal diffusivities respectively.
$\alpha_{t,\,n}$	non-dimensional thermal diffusivity
ΔT	reference temperature difference
ϵ	dissipation
$\overline{\theta}$	non-dimensionalized temperature.
ν, ν_t	laminar and turbulent kinematic viscosity
σ_k, σ_ϵ	turbulence model constants.

Subscript

n	non-dimensional value
o	reference, offset jet
w	wall, wall jet
∞	ambient condition

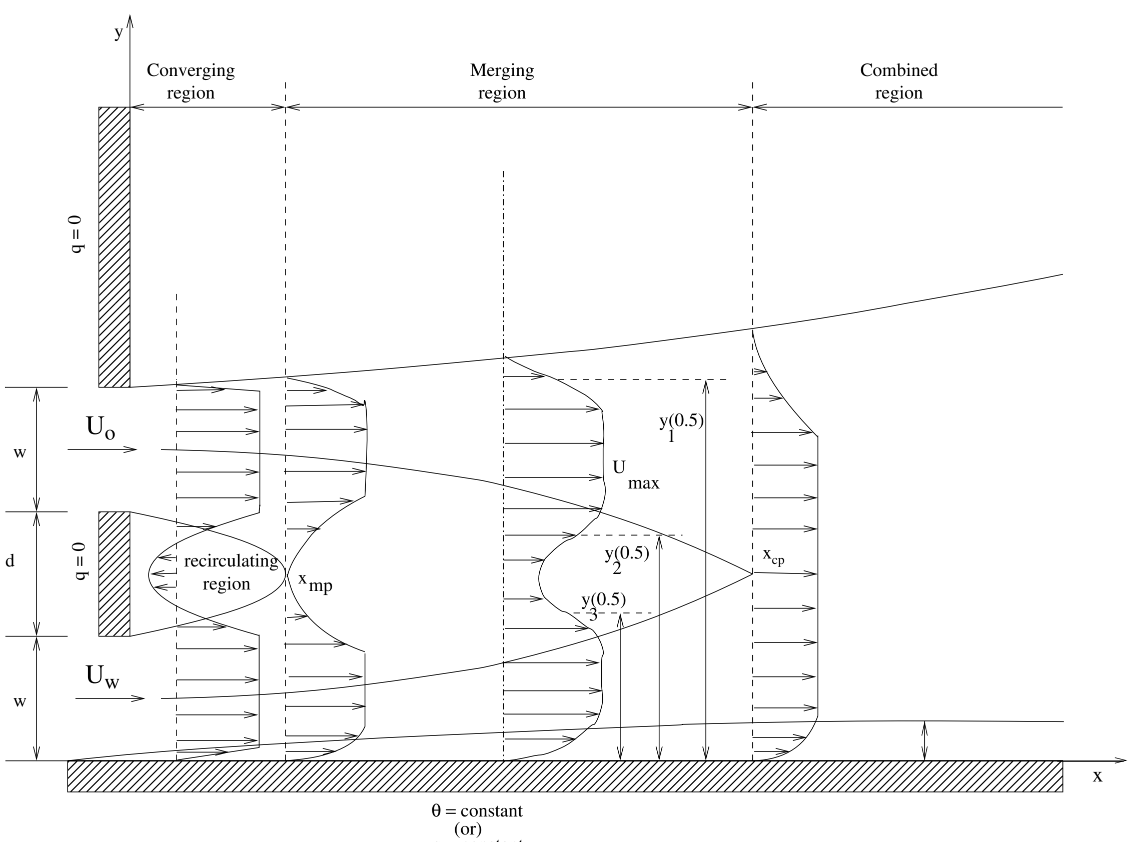

Fig. 1. Schematic diagram of the combined jet flow.

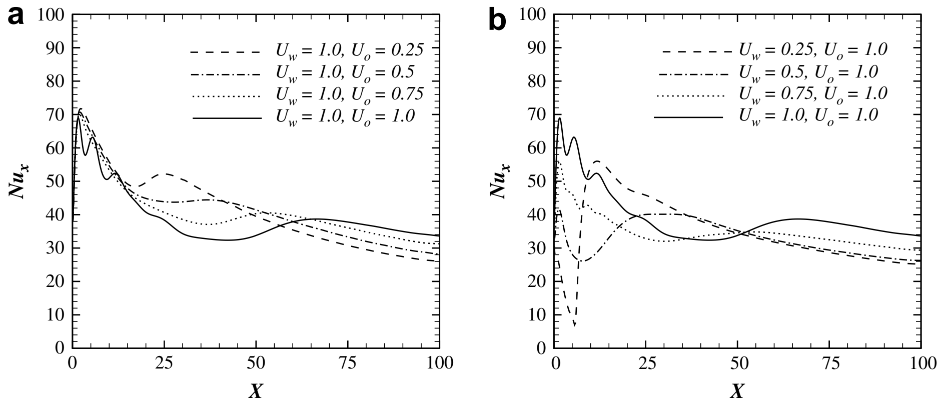

Fig. 2. Variation of Local Nusselt number (Nu_x) along the wall for different wall jet and offset velocities keeping the $Re = 20{,}000$ under constant wall temperature.

Salamah and Kaminski [27]. The jet-to-jet interaction, the geometric parameters of the jet array, and the effect of Reynolds number are investigated. Yilbas et al. [28] studied numerically the jet impingement onto a hole with a constant wall temperature. In the simulations, four hole wall temperatures and two jet velocities were considered. The Nusselt number ratio was computed and the mass flow ratio was determined. However, the heat transfer study of the combined wall jet and offset jet has not been reported. The present study focuses on the effect of combined jets on heat transfer characteristics, particularly when jets are with different mass flow rates. This can be useful in the design of effective heating/cooling systems.

The objective of the present study is a detailed numerical simulation of the heat transfer characteristics of a dual-jet flow for a range of wall jet and offset jet velocities. The offset height has been kept constant at 1. The turbulence modeling has been conducted by the standard high Re k–ϵ model with streamline curvature modification. The study is conducted for constant temperature and constant heat flux at the wall. The Reynolds number is varied between 10,000 and 40,000. $Pr = 0.71$ is taken for all computations. The detailed analysis of the local Nusselt number (Nu_x) distribution, local heat flux (q_x), surface temperature (θ_w), average Nusselt number ($\overline{Nu}$), total heat transfer (Q) are studied both in qualitatively and quantitatively.

2. Mathematical formulation

The flow is assumed to be steady, two-dimensional, turbulent and the fluid is incompressible. Body forces are neglected and the properties are assumed to be constant. Reynolds averaged Navier–Stokes (RANS) equations are used for predicting the turbulent flow. Boussinesq approximation is used to link the Reynolds stresses to the velocity gradients. The variant of standard k–ϵ model to include the streamline curvature effects is used for calculating the turbulent viscosity (ν_t) [29]. By assuming the above conditions, the governing equations in dimensional form can be written as,

Continuity equation:

$$\frac{\partial \bar{u}}{\partial x}+\frac{\partial \bar{v}}{\partial y} = 0 \tag{1}$$

x-momentum equation:

$$\frac{\partial(\bar{u}^2)}{\partial x}+\frac{\partial(\overline{uv})}{\partial y} = -\frac{1}{\rho}\frac{\partial \bar{p}}{\partial x}+\frac{\partial}{\partial x}\left[(\nu+\nu_t)\frac{\partial \bar{u}}{\partial x}-\frac{2}{3}k\right]+\frac{\partial}{\partial y}\left[(\nu+\nu_t)\frac{\partial \bar{u}}{\partial y}\right] \tag{2}$$

y-momentum equation:

$$\frac{\partial(\overline{uv})}{\partial x}+\frac{\partial(\bar{v}^2)}{\partial y} = -\frac{1}{\rho}\frac{\partial \bar{p}}{\partial y}+\frac{\partial}{\partial x}\left[(\nu+\nu_t)\frac{\partial \bar{v}}{\partial x}\right] +\frac{\partial}{\partial y}\left[(\nu+\nu_t)\frac{\partial \bar{v}}{\partial y}-\frac{2}{3}k\right] \tag{3}$$

Energy equation:

$$\frac{\partial(\overline{uT})}{\partial x}+\frac{\partial(\overline{vT})}{\partial y} = \frac{\partial}{\partial x}\left[(\alpha+\alpha_t)\frac{\partial \bar{T}}{\partial x}\right]+\frac{\partial}{\partial y}\left[(\alpha+\alpha_t)\frac{\partial \bar{T}}{\partial y}\right] \tag{4}$$

Turbulent kinetic energy (k) equation:

$$\frac{\partial(\bar{u}k)}{\partial x}+\frac{\partial(\bar{v}k)}{\partial y} = \frac{\partial}{\partial x}\left[\left(\nu+\frac{\nu_t}{\sigma_k}\right)\frac{\partial k}{\partial x}\right] +\frac{\partial}{\partial y}\left[\left(\nu+\frac{\nu_t}{\sigma_k}\right)\frac{\partial k}{\partial y}\right]+G-\epsilon \tag{5}$$

Rate of dissipation (ϵ) equation:

$$\frac{\partial(\bar{u}\epsilon)}{\partial x}+\frac{\partial(\bar{v}\epsilon)}{\partial y} = \frac{\partial}{\partial x}\left[\left(\nu+\frac{\nu_t}{\sigma_\epsilon}\right)\frac{\partial \epsilon}{\partial x}\right]+\frac{\partial}{\partial y}\left[\left(\nu+\frac{\nu_t}{\sigma_\epsilon}\right)\frac{\partial \bar{\epsilon}}{\partial y}\right] +C_{1\epsilon}\frac{\epsilon}{k}G-C_{2\epsilon}\frac{\epsilon^2}{k} \tag{6}$$

Where production by shear (G):

$$G = \nu_t\left[2\left(\frac{\partial \bar{u}}{\partial x}\right)^2+2\left(\frac{\partial \bar{v}}{\partial y}\right)^2+\left(\frac{\partial \bar{u}}{\partial y}+\frac{\partial \bar{v}}{\partial x}\right)^2\right] \tag{7}$$

Eddy viscosity (ν_t) is given as:

$$\nu_t = C_\mu\frac{k^2}{\epsilon} \tag{8}$$

The dimensionless variables are defined as:

$$\bar{U} = \frac{\bar{u}}{U_0},\quad \bar{V} = \frac{\bar{v}}{U_0},\quad \bar{\theta} = \frac{\bar{T}-T_\infty}{\Delta T},\quad X = \frac{\bar{x}}{h},\quad Y = \frac{\bar{y}}{h}, \quad \bar{P} = \frac{\bar{p}-\bar{p}_0}{\rho U_0^2},\quad k_n = \frac{k}{U_0^2},\quad \epsilon_n = \frac{\epsilon}{U_0^3/h},\quad \nu_{t,n} = \frac{\nu_t}{\nu} \tag{9}$$

The non-dimensionalized equations are:

Continuity Equation:

$$\frac{\partial \bar{U}}{\partial X}+\frac{\partial \bar{V}}{\partial Y} = 0 \tag{10}$$

x-momentum equation:

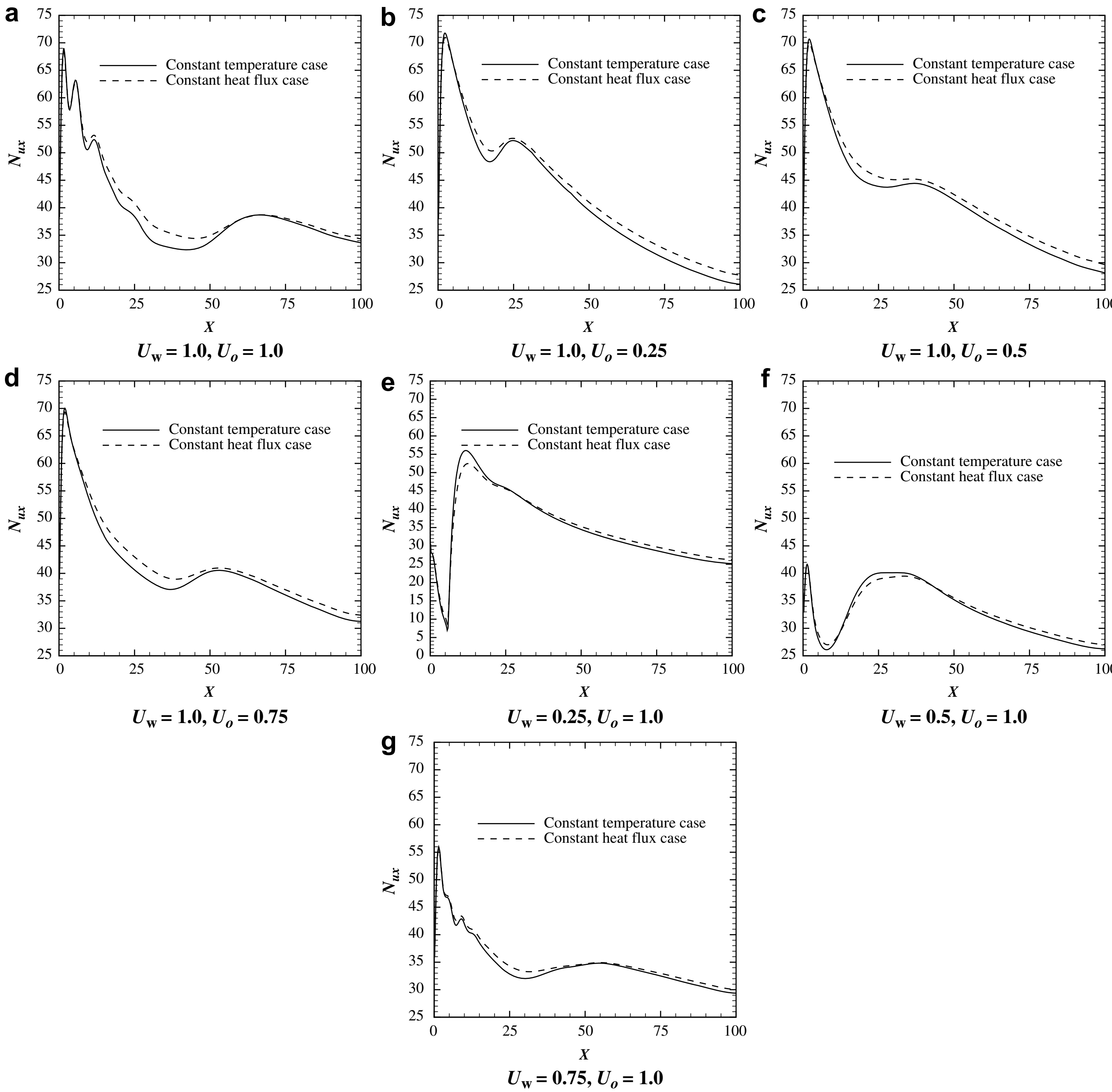

Fig. 3. Comparison of Nu_x along the wall for different wall jet and offset jet velocities for constant wall temperature and constant heat flux cases.

$$\frac{\partial(\overline{U})^2}{\partial X}+\frac{\partial(\overline{UV})}{\partial Y} = -\frac{\partial}{\partial X}\left(\overline{P}+\frac{2}{3}k\right)+\frac{1}{Re}\frac{\partial}{\partial X}\left[(1+\nu_{t,n})\frac{\partial\overline{U}}{\partial X}\right] +\frac{1}{Re}\frac{\partial}{\partial Y}\left[(1+\nu_{t,n})\frac{\partial\overline{U}}{\partial Y}\right] \tag{11}$$

y-momentum equation:

$$\frac{\partial(\overline{UV})}{\partial X}+\frac{\partial(\overline{V})^2}{\partial Y} = -\frac{\partial}{\partial Y}\left(\overline{P}+\frac{2}{3}k\right)+\frac{1}{Re}\frac{\partial}{\partial X}\left[(1+\nu_{t,n})\frac{\partial\overline{V}}{\partial X}\right] +\frac{1}{Re}\frac{\partial}{\partial Y}\left[(1+\nu_{t,n})\frac{\partial\overline{V}}{\partial Y}\right] \tag{12}$$

Energy equation:

$$\frac{\partial(\overline{U\theta})}{\partial X}+\frac{\partial(\overline{V\theta})}{\partial Y} = \frac{1}{Re\cdot Pr}\frac{\partial}{\partial X}\left[(1+\alpha_{t,n})\frac{\partial\overline{\theta}}{\partial X}\right] +\frac{1}{Re\cdot Pr}\frac{\partial}{\partial Y}\left[(1+\alpha_{t,n})\frac{\partial\overline{\theta}}{\partial Y}\right] \tag{13}$$

Turbulent kinetic energy (k_n) equation is:

$$\frac{\partial(\overline{U}k_n)}{\partial X}+\frac{\partial(\overline{V}k_n)}{\partial X} = \frac{1}{Re}\cdot\frac{\partial}{\partial X}\left[\left(1+\frac{\nu_{t,n}}{\sigma_k}\right)\frac{\partial k_n}{\partial X}\right] +\frac{1}{Re}\cdot\frac{\partial}{\partial Y}\left[\left(1+\frac{\nu_{t,n}}{\sigma_k}\right)\frac{\partial k_n}{\partial Y}\right]+G_n-\epsilon_n \tag{14}$$

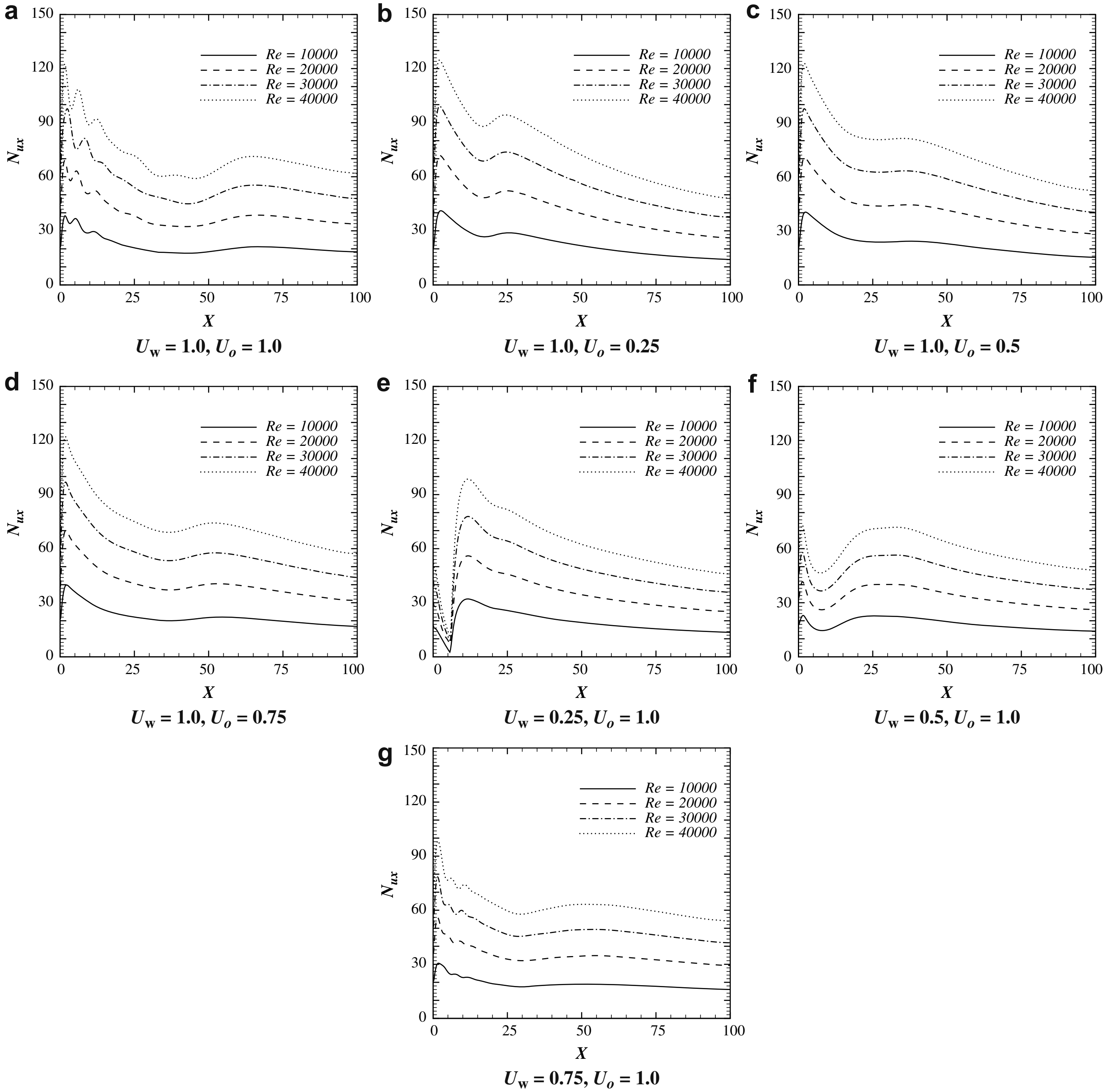

Fig. 4. Local Nusselt number (Nu_x) distribution along the wall for different Reynolds numbers for different wall jet and offset jet velocities under constant temperature case.

Rate of dissipation (ϵ_n) equation is:

$$\frac{\partial(\overline{U}\epsilon_n)}{\partial X}+\frac{\partial(\overline{V}\epsilon_n)}{\partial X} = \frac{1}{Re}\cdot\frac{\partial}{\partial X}\left[\left(1+\frac{\nu_{t,n}}{\sigma_\epsilon}\right)\frac{\partial\epsilon_n}{\partial X}\right]+\frac{1}{Re}\cdot\frac{\partial}{\partial Y}\left[\left(1+\frac{\nu_{t,n}}{\sigma_\epsilon}\right)\frac{\partial\epsilon_n}{\partial Y}\right]+C_{1\epsilon}\frac{\epsilon_n}{k_n}G_n-C_{2\epsilon}\frac{\epsilon_n^2}{k_n} \tag{15}$$

Production (G):

$$G_n = \frac{\nu_{t,n}}{Re}\left[2\left(\frac{\partial\overline{U}}{\partial X}\right)^2+2\left(\frac{\partial\overline{V}}{\partial Y}\right)^2+\left(\frac{\partial\overline{U}}{\partial Y}+\frac{\partial\overline{V}}{\partial X}\right)^2\right] \tag{16}$$

Eddy viscosity ($\nu_{t,\,n}$):

$$\nu_{t,n} = C_\mu Re\frac{k_n^2}{\epsilon_n} \tag{17}$$

The model constants are given as: $\sigma_k = 1.0$, $\sigma_\epsilon = 1.30$, $C_{1\epsilon} = 1.44$, $C_{2\epsilon} = 1.92$, and C_μ is given by Cheng and Farokhi [29] as

$$C_\mu = \frac{2\phi}{3}\left[1-R_f-\phi\frac{G_n}{\epsilon}\,\frac{R_f^2+4R_f+1}{1-R_f}\right] \tag{18}$$

Where R_f is called the flux Richardson number

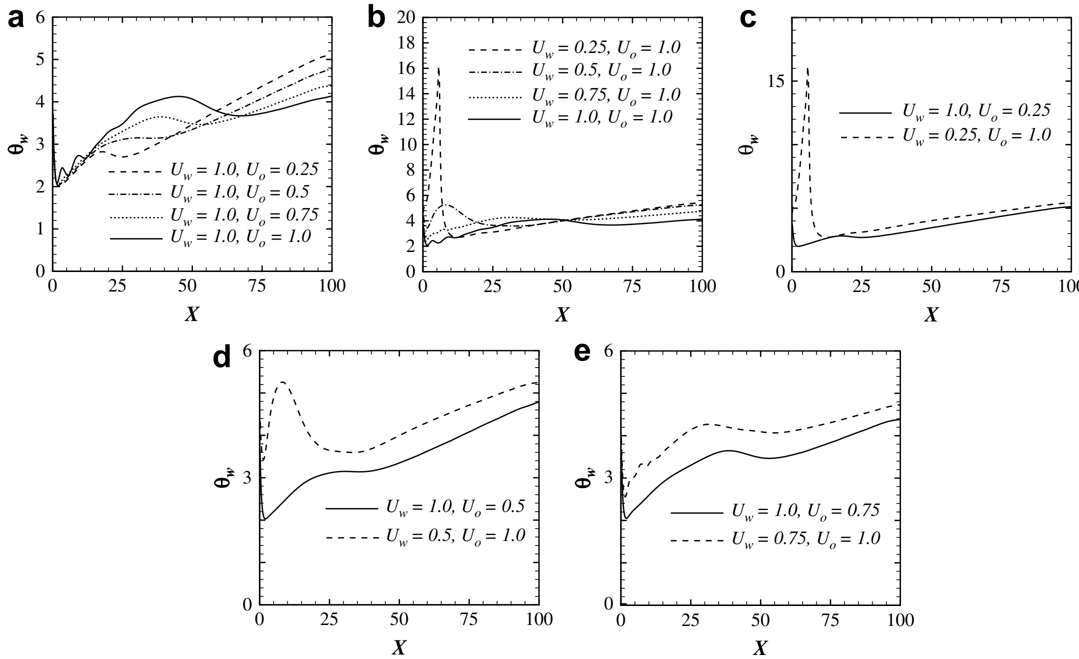

Fig. 5. Variation of temperature (θ) along the wall for different wall jet and offset velocities keeping $Re = 20{,}000$ under constant wall heat flux.

$$R_f = \frac{\partial \overline{V}/\partial X}{\partial \overline{U}/\partial Y}$$

ϕ is defined as:

$\phi = 1 - C_b/C_a - 1 + G_n/\epsilon$ where, $C_a = 1.5$ and $C_b = 0.76$

2.1. Boundary conditions

The flow of a combined wall jet and offset jet emanating into the quiescent fluid is considered. Since the governing equations are non-dimensionalized, the boundary conditions are also non-dimensionalized and given as the input to the solution. The inlets of combined jet, U_w and U_o represents the non-dimensional wall jet and offset jet velocities respectively. In the present study, keeping $U_w = 1.0$, U_o is varied for 0.25, 0.5, 0.75 and 1.0. Similarly, keeping $U_o = 1.0$, U_w is varied for 0.25, 0.5, 0.75 and 1.0, which totally represents seven possible combinations. For the turbulent kinetic energy equation, the boundary condition at inlets is $k_n = 1.5I^2$ where I is the turbulence intensity and is equal to 0.02. For the dissipation equation, the boundary condition is $\epsilon_n = (k_n^{3/2} C_\mu^{3/4})/l$, where $l = 0.07h$ is considered. For the solid wall, no slip boundary condition is considered for velocity. Neumann boundary conditions are provided for the top boundary (i.e. entrainment side) and at the exit boundary, a developed condition of $\partial\phi/\partial n = 0$ is considered where $\phi = \overline{U}, \overline{v}, k_n, \epsilon_n$ and θ. It has been ensured that the first grid point near the wall falls in the logarithmic region i.e. $30 < Y^+ < 100$ where $Y^+ = yu_\tau/\nu$, u_τ being the friction velocity. For constant temperature case, wall temperature is $\theta = 1$ whereas for constant flux case, $q_x = \text{constant}$. For both the cases, θ at inlet and the entrainment boundary is 0.

3. Numerical scheme and method of solution

In the present work, the dimensionless governing equations are discretized using the control volume method [30]. The power-law scheme is used to discretize the convective terms and the central difference is used for diffusive terms due to ensure the stability of the solution. To avoid the fine mesh required to resolve the viscous sub-layer near the boundary, wall function method [31] has been used which is appropriate for high Reynolds number flows. SIMPLE [30] algorithm is followed to couple the velocity and pressure. Pseudo-transient approach [32] is used to under-relax the momentum and the turbulent equations. An under-relaxation of 0.2 is used for pressure. Euclidean norm of residual is used to calculate the momentum residuals along with mass imbalance. The Euclidean norm is used for calculating the residual. The residuals calculated for all the variables and the cases considered are of the order of 10^{-4}, which is considered to be optimum for the convergence.

3.1. Code validation and grid independence study

To validate the code developed, the steady-state computations are performed for $U_w = U_o = 1.0$ and $Re = 10{,}000$ is considered. The similarity solution of the $\overline{U}$ velocity profile at $X = 15$, 25 and 30 downstream locations respectively are compared with experimental results of Wang and Tan [24] and are in good agreement with the similarity solution of experimental study. In order to assess the difference between the standard k–ϵ model and its streamline curvature (SC) modification, the results of both are compared to the experimental solution. It is observed that the streamline curvature modification gives the better results. The maximum velocity decay in the downstream direction are compared for SC modified k–ϵ with the experimental study. In the present computation, the computed results slightly over-predicts with the experimental solution. The outer boundary layer growth is compared and, the results are in good agreement with experimental solution. The details of the comparison are given in Vishnuvardhanarao and Das [33].

A detailed study has been conducted to find out the grid independence and the domain size for the solution to be independent. It is found that the grid size of 201×141 is acceptable. The size of the domain is 100 in the X-direction and 50 in the Y-direction. The details of the grid independence study are also given in Vishnuvardhanarao and Das [33].

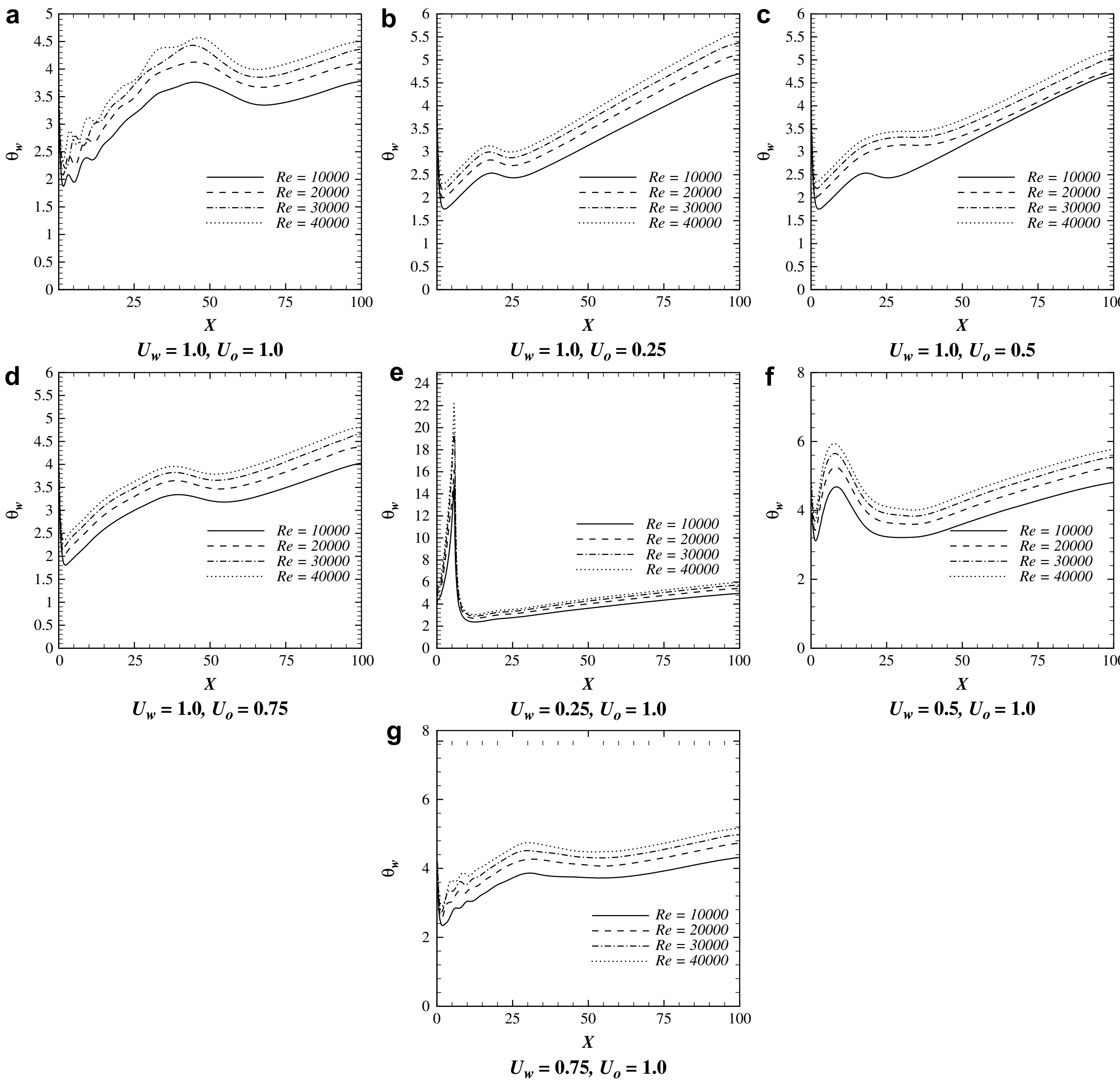

Fig. 6. Temperature (θ) distribution along the wall for different Reynolds numbers for different wall jet and offset jet velocities under constant wall heat flux.

4. Results and discussion

The present study can be briefly classified into two cases. Those are (1) keeping the wall jet velocity ($U_w = 1.0$) constant, offset jet velocity (U_o) is varied for 0.25, 0.5 and 0.75. (2) keeping offset jet velocity ($U_o = 1.0$) constant, wall jet velocity is varied for 0.25, 0.5, 0.75 and 1.0. Reynolds number is varied from 1×10^4 to 4×10^4 for a constant Prandtl number ($Pr = 0.71$). The increase in the Reynolds number can be inferred as increasing the jet velocities while maintaining the same velocity ratio. Two cases of the solid wall boundary conditions are considered: viz. constant wall temperature and constant wall heat flux. Under these conditions, the heat transfer study is carried out for local Nusselt number (Nu_x) distribution, local heat flux (q_x) and surface temperature distribution (θ_w) along the wall.

4.1. Local Nusselt number

The Nu_x distribution along the wall for different wall and offset jet velocities, keeping the $Re = 2 \times 10^4$ is shown in Fig. 2. Fig. 2(a) demonstrates the case for $U_w = 1.0$ and varying the U_o. For $U_o = 1.0$, the fluctuations in the Nu_x near the inlet can be viewed as vortex shedding as observed in Wang and Tan [24] along the wall up to $X \cong 15$. Beyond this region, the flow is observed to be steady. Near the inlet, local Nusselt number (Nu_x) is almost same for all U_o except for $U_o = 1.0$ up to $X \cong 20$. Hence, it can be inferred that U_o has very little influence on the local Nusselt number up to $X \cong 20$. It can be observed from Fig. 2(a) that, for $U_o = 0.25$, the Nu_x is maximum at the inlet and decreases up to some point say, $P_1(X \cong 20)$ in the downstream. Further downstream, there is an increase in Nu_x up to point say, $P_2(X \cong 30)$ and beyond which it decreases continuously.

Table 1
Average Nusselt number ($\overline{Nu}$) and total heat transfer (Q) at different Re, keeping the $U_w = 1.0$ and varying U_o.

	B.C	Re	$U_o = 0.25$	$U_o = 0.5$	$U_o = 0.75$	$U_o = 1.0$
$\overline{Nu}$	$\theta_w = C$	10^4	30.3388(5.367)	30.1936(4.863)	29.7268(3.241)	28.7934
		2×10^4	55.0086(5.128)	54.9122(4.944)	54.2049(3.592)	52.3252
		3×10^4	77.8658(4.606)	77.8354(4.564)	76.9002(3.308)	74.4378
		4×10^4	99.5772(4.564)	99.6774(4.984)	98.6782(3.62)	95.2309
	$q_w = C$	10^4	31.5061(5.876)	31.5061(5.876)	30.7894(3.468)	29.7574
		2×10^4	56.7962(5.573)	56.617(5.24)	55.8176(3.754)	53.7978
		3×10^4	80.145(4.967)	80.0039(4.782)	78.9511(3.403)	76.3527
		4×10^4	102.288(4.985)	102.247(4.943)	101.092(3.758)	97.4308
Q	$\theta_w = C$	10^4	0.320481(5.367)	0.318947(4.863)	0.314015(3.241)	0.304156
		2×10^4	0.290539(5.128)	0.290029(4.943)	0.286294(3.592)	0.276366
		3×10^4	0.274175(4.605)	0.274068(4.562)	0.270775(3.307)	0.262105
		4×10^4	0.262968(4.563)	0.263232(4.669)	0.260594(3.62)	0.25149

Table 2
Average Nusselt number ($\overline{Nu}$) and total heat transfer (Q) at different Re, keeping the $U_o = 1.0$ and varying U_w.

	B.C	Re	$U_w = 0.25$	$U_w = 0.5$	$U_w = 0.75$	$U_w = 1.0$
$\overline{Nu}$	$\theta_w = C$	10^4	25.6966(−10.755)	24.4261(−15.167)	25.5035(−11.426)	28.7934
		2×10^4	46.2771(−11.558)	44.0201(−15.872)	46.2877(−11.538)	52.3252
		3×10^4	65.1709(−12.45)	62.0621(−16.626)	65.6028(−11.869)	74.4378
		4×10^4	83.1486(−12.687)	79.215(−16.818)	83.8711(−11.928)	95.2309
	$q_w = C$	10^4	26.0511(−12.455)	24.6294(-17.232)	26.0526(−12.45)	29.7574
		2×10^4	46.644(−13.297)	44.2912(-17.671)	47.0871(−12.474)	53.7978
		3×10^4	65.5673(−14.126)	62.3684(−18.315)	66.5912(−12.785)	76.3527
		4×10^4	83.5845(−14.211)	79.5426(−18.36)	85.0345(−12.723)	97.4308
Q		10^4	0.2714(−10.755)	0.2580(−15.167)	0.2694(−11.426)	0.3041
		2×10^4	0.2444(−11.558)	0.2325(−15.872)	0.2444(−11.538)	0.2763
		3×10^4	0.2294(−12.449)	0.2185(−16.625)	0.2309(−11.868)	0.2621
		4×10^4	0.2195(−12.687)	0.2091(−16.817)	0.2214(−11.928)	0.2515

Table 3
% change in $\overline{Nu}$ and Q when the Re is increased at different wall jet and offset jet velocities.

		Re	$U_w = 1, U_o = 0.25$	$U_w = 1, U_o = 0.5$	$U_w = 1, U_o = 0.75$	$U_w = 0.25, U_o = 1.0$	$U_w = 0.5, U_o = 1.0$	$U_w = 0.75, U_o = 1.0$	$U_w = 1.0, U_o = 1.0$
$\overline{Nu}$	$\theta_w = C$	10^4	30.3388	30.1936	29.7268	25.6966	24.4261	25.5035	28.7934
		2×10^4	55.0086(81.3)	54.9122(81.8)	54.2049(82.3)	46.2771(80.1)	44.0201(80.2)	46.2877(81.5)	52.3252(81.7)
		3×10^4	77.8658(156.7)	77.8354(157.7)	76.9002(158.6)	65.1709(153.6)	62.0621(154.1)	65.6028(157.2)	74.4378(158.5)
		4×10^4	99.5772(228.2)	99.6774(230.1)	98.6782(231.9)	83.1486(223.6)	79.215(224.3)	83.8711(228.8)	95.2309(230.7)
	$q_w = C$	10^4	31.5061	31.5061	30.7894	26.0511	24.6294	26.0526	29.7574
		2×10^4	56.7962(83.4)	56.617(79.7)	55.8176(81.2)	46.644(79)	44.2912(79.8)	47.0871(80.7)	53.7978(80.7)
		3×10^4	80.145(159.4)	80.0039(153.9)	78.9511(156.4)	65.5673(151.7)	62.3684(153.2)	66.5912(155.6)	76.3527(156.6)
		4×10^4	102.288(224.6)	102.247(224.5)	101.092(228.3)	83.5845(220.8)	79.5426(222.9)	85.0345(226.4)	97.4308(227.4)
Q	$\theta_w = C$	10^4	0.320	0.318	0.314	0.271	0.258	0.269	0.304
		2×10^4	0.290(−9.34)	0.290(−9.06)	0.286(−8.82)	0.244(−9.95)	0.2325(−9.89)	0.2444(−9.25)	0.2763(−9.13)
		3×10^4	0.274(−14.48)	0.274(−14.07)	0.270(−13.77)	0.229(−15.46)	0.218(−15.30)	0.230(−14.25)	0.262(−13.82)
		4×10^4	0.262(−17.94)	0.263(−17.46)	0.260(−17.01)	0.219(−19.10)	0.209(−18.92)	0.221(−17.78)	0.251(−17.31)

Similar trends are observed for other values of U_o (Fig. 2(a)). However, as the value of U_o increases, the corresponding points P_1 and P_2 shift towards downstream and the distance between them also widens. This is because of the delay in jet-mixing and the formation of a wall jet. The increase in Nu_x between points P_1 and P_2 (for all values of U_o) can be due to the influence of mixing of two streams and development of self-similarity. In far downstream ($X \geq 60$), Nu_x is larger as the offset jet velocity increases.

The variation of Nu_x with U_w at constant U_o (=1.0) is shown in Fig. 2(b). At the inlet Nu_x increases with U_w, which suggests that the wall jet velocity has considerable influence as compared to the offset jet velocity. As the wall jet velocity is less, the offset jet predominates and Nu_x is less because of the relative strength of the recirculation bubble. For values of $U_w > 0.5$, the maximum Nu_x occurs near the inlet and for values of $U_w < 0.5$, the maximum Nu_x occurs at some point in the downstream. It is found that for $U_w = 0.25$, Nu_x decreases to very low compared to other U_w and then rapidly increases to maximum value. Similar trend can be observed for $U_w = 0.5$, but increases slowly compared to $U_w = 0.25$. For values of $U_w = 0.75$ and 1.0 at constant U_o, the trends are similar to the constant U_w as seen in Fig. 2(a). In the far downstream ($X \geq 60$), Nu_x increases as the wall jet velocity increases. When the Nu_x distribution is compared for different U_w and U_o by interchanging them, it is observed that almost in the entire flow domain, Nu_x is more when the $U_w > U_o$. Near the inlet, the difference in Nu_x is found more, but this difference in Nu_x decreases as the distance from the inlet increases and finally becomes equal which states that it depends on the total mass flow rate.

The comparison of Nu_x distribution at the wall for different U_w and U_o under constant heat flux and constant temperature

Table 4
% of change in Nu and Q when $U_w = 0.25$, $U_o = 1.0$ and interchanging the velocities.

	B.C	Re	$U_w = 0.25$, $U_o = 1.0$	$U_w = 1.0$, $U_o = 0.25$	% Increase
$\overline{Nu}$	$\theta_w = C$	10^4	25.6966	30.3388	18.052
		2×10^4	46.2771	55.0086	18.867
		3×10^4	65.1709	77.8658	19.479
		4×10^4	83.1486	99.5772	19.758
	$q_w = C$	10^4	26.0511	31.5061	20.939
		2×10^4	46.644	56.7962	21.765
		3×10^4	65.5673	80.145	22.233
		4×10^4	83.5845	102.288	22.376
Q	$\theta_w = C$	10^4	0.271443	0.320481	18.065
		2×10^4	0.244421	0.290539	18.868
		3×10^4	0.229475	0.274175	19.479
		4×10^4	0.219583	0.262968	19.579

Table 6
% of increase in Nu and Q when $U_w = 0.75$, $U_o = 1.0$ and interchanging the velocities.

	B.C	Re	$U_w = 0.75$, $U_o = 1.0$	$U_w = 1.0$, $U_o = 0.75$	% Increase
$\overline{Nu}$	$\theta_w = C$	10^4	25.5035	29.7268	16.559
		2×10^4	46.2877	54.2049	17.104
		3×10^4	65.6028	76.9002	17.221
		4×10^4	83.8711	98.6782	17.655
	$q_w = C$	10^4	26.0526	30.7894	18.187
		2×10^4	47.0871	55.8176	18.541
		3×10^4	66.5912	78.9511	18.561
		4×10^4	85.0345	101.092	18.883
Q	$\theta_w = C$	10^4	0.269403	0.314015	16.559
		2×10^4	0.244477	0.286294	17.105
		3×10^4	0.230996	0.270775	17.221
		4×10^4	0.221491	0.260594	17.654

conditions applied at the wall is shown in Fig. 3. As it demonstrates, though the Nu_x is slightly more under constant heat flux condition, the behavior is almost the same.

Fig. 4 shows the variation of Nu_x with Reynolds number along the wall when the wall temperature is constant. It clearly shows that at all locations in the flow domain, as Re is increased Nu_x is increased, but no change in the behavior is observed. In contrast to Fig. 4(a)–(d), it is observed that near the inlet, there is a sharp decline in the value of Nu_x when $U_w = 0.25$ keeping $U_o = 1.0$ (refer Fig. 4(e)). It shows that the wall jet velocity is not able to overcome the effect of the recirculation bubble occurring due to the offset jet. The Nu_x value increases near the reattachment point and gradually decreases with a typical characteristics of the wall jet flows. However, as U_w is gradually increased (Fig. 4(f), (g)), the wall jet increases in strength with a desirable increase in Nu_x. As Fig. 3 suggests, a similar phenomenon is found in the case of constant wall heat flux also.

4.2. Wall temperature distribution

The variation in wall temperature (θ_w), which occurs in the case of constant heat flux condition is shown in Fig. 5. Fig. 5(a) shows the variation of θ_w with U_o at constant $U_w = 1.0$. The wall temperature (θ_w) is same for all values of U_o except $U_o = 1.0$ up to a distance of $X \cong 20$. Further downstream (the region in which the local Nusselt number increases as shown in Fig. 2 between the points P_1 and P_2), the wall temperature decreases due to the increase in heat transfer up to point P_2 beyond which the temperature increases. In the far downstream ($X \geq 60$), at any location θ_w is more when U_o is less. The θ_w distribution with U_w at constant $U_o = 1.0$ is shown in Fig. 5(b). A sharp rise in the wall temperature in the case of $U_w = 0.25$ near inlet can be observed which is obvious due to the steep reduction in the local Nusselt number as seen in Fig. 2(a). As explained earlier, the wall jet velocity is small and is unable to overcome the effect of the offset jet causing the recirculation bubble near the inlet. In the far downstream region, at any location θ_w decreases as the U_w increases. Fig. 5(c)–(e) shows the variation of θ_w when U_w and U_o are interchanged. As it demonstrates, the surface temperature is found more when $U_w < U_o$. It can be concluded from the above observations that the local Nusselt number and the wall temperature are complementary to each other. It is observed that as Re is increased θ_w increases, but no change in its behavior is found in Fig. 6. The difference in θ_w between any two consecutive Re reduces as Re increases.

Table 5
% of change in Nu and Q when $U_w = 0.5$, $U_o = 1.0$ and interchanging the velocities.

	B.C	Re	$U_w = 0.5$, $U_o = 1.0$	$U_w = 1.0$, $U_o = 0.5$	% Increase
$\overline{Nu}$	$\theta_w = C$	10^4	24.4261	30.1936	23.612
		2×10^4	44.0201	54.9122	24.743
		3×10^4	62.0621	77.8354	25.415
		4×10^4	79.215	99.6774	25.831
	$q_w = C$	10^4	24.6294	31.5061	27.921
		2×10^4	44.2912	56.617	27.829
		3×10^4	62.3684	80.0039	28.276
		4×10^4	79.5426	102.247	28.543
Q	$\theta_w = C$	10^4	0.258023	0.318947	23.611
		2×10^4	0.2325	0.290029	24.743
		3×10^4	0.218529	0.274068	25.414
		4×10^4	0.209195	0.263232	25.831

4.3. Average Nusselt number and the total heat transfer

In order to quantify the results, the average Nusselt number ($\overline{Nu}$) and the total heat transfer (Q) are tabulated in Tables 1–6 for constant temperature ($\theta_w = C$) and constant heat flux ($q_x = C$) conditions. Table 1 shows the variation of $\overline{Nu}$ and Q with U_o at constant $U_w = 1.0$. The value within the parenthesis shows the percentage change of $\overline{Nu}$ and Q with $U_o = 1.0$ as the reference value. It is noticed that $\overline{Nu}$ decreases with increase in U_o at all values of Re. Though the $\overline{Nu}$ increases as Re increases, the percentage change with the reference value ($U_o = 1.0$) is fairly constant. At any Re, $\overline{Nu}$ is more for the constant heat flux condition compared to the constant wall temperature condition, however the trends are observed to be same. It is found that the total heat transfer (Q) decreases with U_o and Re. It is observed that there is a decrease in heat flux though Nu_x increases with Re, which is due to the increase in the reference heat flux ($\rho c_p U_o \Delta T$). Table 2 shows the variation of $\overline{Nu}$ and Q with U_w at constant $U_o = 1.0$. The value within the parenthesis shows the percentage change with the reference value of $U_w = 1.0$. It is observed that $\overline{Nu}$ is maximum at $U_w = 1.0$ and minimum at $U_w = 0.5$. A decrease of 15 percent in $\overline{Nu}$ is observed for $U_w = 0.5$. For any Reynolds number, $\overline{Nu}$ is more in the case of constant heat flux compared to the constant wall temperature condition. It is noticed that the total heat transfer decreases with Re. The variation of $\overline{Nu}$ and Q at all wall jet and offset jet velocities with Re is shown in Table 3. In this case $Re = 10^4$ is taken as the reference to evaluate the percentage change which is given in the parenthesis. It is observed that for any U_w and U_o, $\overline{Nu}$ increases almost linearly with Re. An increase in $\overline{Nu}$ by nearly 230% is observed as Re is increased to 4×10^4. However, the non-dimensional Q is observed to decrease by 17 percent. Tables 4–6 show the $\overline{Nu}$ and Q when the U_w and U_o are interchanged. In order to calculate the percentage change, the value of $U_w = 1.0$ condition is considered as reference value. It is observed that both $\overline{Nu}$ and Q are more for $U_w = 1.0$ compared to the case in which $U_o = 1.0$. The maximum percentage change is found in the case of $U_w = 1.0$ and $U_o = 0.5$.

5. Conclusions

The heat transfer study of combined wall jet and offset jet flow is considered. Different wall jet and offset velocities are considered. Analysis is carried out in the graphical form for local Nusselt number (Nu_x), local heat flux (q_x), wall temperature (θ_w) and in tabular form for average heat transfer ($(\overline{Nu})$) and total heat transfer (Q) for constant temperature and constant heat flux conditions. $Pr = 0.71$ is taken for all computations. The important conclusions may be drawn are as follows:

- In the far downstream region, the Nu_x increases with mass flow rate, i.e. by increasing either the wall jet or offset velocity keeping the other constant.
- At the same mass flow rate, when the U_w and U_o are interchanged, the Nu_x is more when the $U_w = 1.0$. In the far downstream location, the Nu_x is same irrespective of the jet velocities.
- As Re is increased, Nu_x is increased for all U_o and U_w, but no change in the behavior is observed.
- Comparison of two boundary conditions (i.e. constant temperature and constant heat flux conditions) Nu_x is more in case of constant heat flux condition.
- When the jet velocities are interchanged, θ_w is more when $U_w < U_o$. As Re increased at any location in the flow domain, θ_w also increased.
- Average Nusselt number is found to be maximum in the case of $U_o = 0.25$ and $U_w = 1.0$ which is 5% higher than the reference. The percentage of change in $\overline{Nu}$ decreases with Re.
- Approximately linear increase in percent of change with Re suggests that the $\overline{Nu}$ increases linearly. Approximately 230 percent increase is observed as Re is increased from 10^4 to 4×10^4.

Acknowledgement

The helpful comments of the reviewers are gratefully acknowledged.

Appendix A. Deriving the expression for Nusselt number calculation

$$Nu_x = \frac{h_c H}{k} = h_c(\overline{T}_w - T_\infty) \times \frac{\nu}{\alpha} \cdot \frac{1}{\rho C_p} \cdot \frac{1}{U_0(\overline{T}_w - T_\infty)} \cdot \frac{U_0 H}{\nu} \tag{19}$$

$$Nu_x = \frac{q_x Pr Re}{\rho C_p U_0(\overline{T}_w - T_\infty)} \tag{20}$$

We can write the above equation as:

$$Nu_x = \frac{q_x Pr Re}{\rho C_p U_0(\overline{T}_w - T_\infty)} \cdot \frac{\Delta T}{\Delta T} \tag{21}$$

where ΔT is $(\overline{T}_w - T_\infty)$ for constant wall temperature case and $q_c/\rho c_p U_0$ for constant heat flux case Finally:

$$Nu_x = \frac{q_{x,n} Pr Re}{\overline{\theta}_w}. \tag{22}$$

since $\overline{\theta}_\infty = 0$. The above procedure is obtained as mentioned in reference [34], which is used for calculating the local Nusselt number distribution. The average Nusselt number is calculated as:

$$\overline{Nu} = \frac{1}{L}\int_0^L Nu_x dx \tag{23}$$

Heat flux at the wall is given by [32]:

$$q_{x,n} = \frac{(\overline{\theta}_w - \overline{\theta}_p) c_\mu^{\frac{3}{4}} k_n^{\frac{1}{2}}}{Pr_t\left(\frac{1}{\kappa}\log\left(EY^+\right) + P_f\right)} \tag{24}$$

where θ_p is the temperature at the first grid point near wall and P_f is the pee-function, which is given by:

$$P_f = 9.24\left[\left(\frac{Pr}{Pr_t}\right)^{\frac{3}{4}} - 1\right] \times \left[1 + 0.28\exp\left(-0.007\frac{Pr}{Pr_t}\right)\right] \tag{25}$$

The non-dimensional total heat transfer (Q) at the wall is calculated as:

$$Q = \frac{1}{L}\int_0^L q_{x,n} dx \tag{26}$$

References

[1] M.B. Glauert, The wall jet, Journal of Fluid Mechanics 1 (1956) 625–643.
[2] D.J. Tritton, Physical Fluid Dynamics, Von Norstrand Reinhold, UK, 1977, pp. 284–286.
[3] P. Bakke, An experimental investigation of a wall jet, Journal of Fluid Mechanics 2 (1957) 467–472.
[4] W.H. Schwarz, W.P. Cosart, The two-dimensional turbulent wall-jet, Journal of Fluid Mechanics 10 (1961) 481–495.
[5] I. Wygnanski, Y. Katz, E. Horev, On the applicability of various scaling laws to the turbulent wall jet, Journal of Fluid Mechanics 234 (1992) 669–690.
[6] B.E. Launder, W. Rodi, The turbulent wall jet-measurements and modeling, Annual Review of Fluid Mechanics 15 (1983) 429–459.
[7] J.G. Eriksson, R.I. Karlsson, J. Persson, An experimental study of a two-dimensional plane turbulent wall jet, Experiments in Fluids 25 (1998) 50–60.
[8] B. Venås, H. Abrahamsson, P.Å. Krogstad, L. Löfdahl, Pulsed hot-wire measurements in two- and three-dimensional wall jets, Experiments in Fluids 27 (1999) 210–218.
[9] S. Gogineni, C. Shih, Experimental investigation of the unsteady structure of a transitional plane wall jet, Experiments in Fluids 23 (1997) 121–129.
[10] W.K. George, H. Abrahamsson, J. Eriksson, R.I. Karlsson, L. Löfdahl, M. Wosnik, A similarity theory for the turbulent plane wall jet without external stream, Journal of Fluid Mechanics 425 (2000) 367–411.
[11] J.R.R. Pelfrey, J.A. Liburdy, Effect of curvature on the turbulence of a two-dimensional jet, Experiments in Fluids 4 (1986) 143–149.
[12] H.-M. Koo, S.O. Park, Prediction of turbulent offset jet flows with an assessment of QUICKER scheme, International Journal for Numerical Methods in Fluids 15 (1992) 355–372.
[13] J.R.R. Pelfrey, J.A. Liburdy, Mean flow characteristics of a turbulent offset jet, Transaction ASME: Journal of Fluids Engineering 108 (1986) 82–88.
[14] R. Gu, Modelling two-dimensional turbulent offset jets, Journal of Hydraulic Engineering 122 (11) (1996) 617–624.
[15] R.A. Sawyer, The flow due to a two-dimensional jet issuing parallel to a flat plate, Journal of Fluid Mechanics 9 (1960) 543–559.
[16] R.A. Sawyer, Two-dimensional reattaching jet flows including the effects of curvature on entrainment, Journal of Fluid Mechanics 17 (1963) 481–498.
[17] A. Nasr, J.C.S. Lai, A turbulent plane offset jet with small offset ratio, Experiments in Fluids 24 (1998) 47–57.
[18] N.W.M. Ko, K.K. Lau, Flow structures in initial region of two interacting parallel plane jets, Experimental Thermal Fluid Sciences 2 (1989) 431–449.
[19] Y.F. Lin, M.J. Sheu, Investigation of two plane parallel unventilated jets, Experiments in Fluids 10 (1990) 17–22.
[20] A. Nasr, J.C.S. Lai, Comparison of flow characteristics in the near field of two parallel plane jets and an offset jet, Physics of Fluids 9 (1997) 2919–2931.
[21] C.Y. Soong, P.Y. Tzeng, C.D. Hsieh, Numerical investigation of flow structure and bifurcation phenomena of confined plane twin-jet flows, Physics of Fluids 10 (1998) 2910–2921.
[22] E.A. Anderson, R.E. Spall, Experimental and numerical investigation of two-dimensional parallel jets, Transaction ASME: Journal of Fluids Engineering 123 (2001) 401–406.
[23] C.S. Wang, Y.F. Lin, M.J. Sheu, Measurements of turbulent inclined plane dual jets, Experiments in Fluids 16 (1993) 27–35.
[24] K. .Wang, S.K. Tan, Experimental investigation of the interaction between a plane wall jet and a parallel offset jet, Experiments in Fluids 42 (2007) 551–562.
[25] S.Z. Shuja, B.S. Yilbas, M.O. Budair, Gas jet impingement on a surface having a limited constant flux area: various turbulence models, Numerical Heat Transfer: Part A 36 (2) (1999) 171–200.

[26] L.B.Y. Aldabbagh, I. Sezai, Numerical simulation of three-dimensional laminar, square twin-jet impingement on a flat plate, flow structure and heat transfer, Numerical Heat Transfer: Part A 41 (8) (June 2002) 835–850.
[27] S.A. Salamah, D.A. Kaminski, Modeling of turbulent heat transfer from an array of submerged jets impinging on a solid surface, Numerical Heat Transfer: Part A 48 (4) (2005) 315–337.
[28] B.S. Yilbas, S.Z. Shuja, M.O. Budair, Jet impingement onto a hole with constant wall temperature, Numerical Heat Transfer: Part A 43 (8) (2003) 843–865.
[29] G.C. Cheng, S. Farokhi, On turbulent flows dominated by curvature effects, ASME: Journal of Fluids Engineering 114 (1992) 52–57.
[30] S.V. Patankar, Numerical Heat Transfer and Fluid Flow, Hemisphere, New York, 1980.
[31] B.E. Launder, D.B. Spalding, The numerical computation of turbulent flows, Computer Methods in Applied Mechanics and Engineering 3 (1974) 269–289.
[32] H.K. Versteeg, W. Malalasekera, An Introduction to Computational Fluid Dynamics. The Finite Volume Method, LONGMAN, 1996.
[33] E. Vishnuvardhanarao, M.K. Das, Numerical simulation of the turbulent flow interaction between a plane wall jet and a parallel offset jet, Applied Mathematical Modelling, submitted for publication.
[34] G. Biswas, The k–ϵ model, the RNG k–ϵ model and the phase-averaged model, in: G. Biswas, V. Eswaran (Eds.), Turbulent Flows: Fundamentals, Experiments and Modeling, Chapter 11, Narosa Publishing House, New Delhi, India, 2002, pp. 339–375.